



Jet Propulsion Laboratory
California Institute of Technology

CGI Observing Scenario 11 Modeling Results

John Krist

Jet Propulsion Laboratory
California Institute of Technology
Pasadena, CA 91109

August 26 – 27, 2024

• NASA GODDARD SPACE FLIGHT CENTER • JET PROPULSION LABORATORY •
• L3HARRIS TECHNOLOGIES • BALL AEROSPACE • TELEDYNE • NASA KENNEDY SPACE CENTER •
• SPACE TELESCOPE SCIENCE INSTITUTE • INFRARED PROCESSING AND ANALYSIS CENTER •
• EUROPEAN SPACE AGENCY • JAPAN AEROSPACE EXPLORATION AGENCY •
• CENTRE NATIONAL d'ÉTUDES SPATIALES • MAX PLANCK INSTITUTE FOR ASTRONOMY •

Copyright 2024 California Institute of Technology.
Government sponsorship acknowledged

JATIS Journal of
Astronomical Telescopes,
Instruments, and Systems

RESEARCH PAPER

**End-to-end numerical modeling of the Roman
Space Telescope coronagraph**

John E. Krist,^{a,*} John B. Steeves^{a,b}, Brandon D. Dube,^a A J Eldorado Riggs^a,
Brian D. Kern,^a David S. Marx,^a Eric J. Cady,^a Hanying Zhou,^a
Ilya Y. Poberezhskiy,^a Caleb W. Baker,^a James P. McGuire,^a Bijan Nemati^{a,c},
Gary M. Kuan,^a Bertrand Mennesson,^a John T. Trauger,^a Navtej S. Saini^a, and
Sergi Hildebrandt Rafels^a

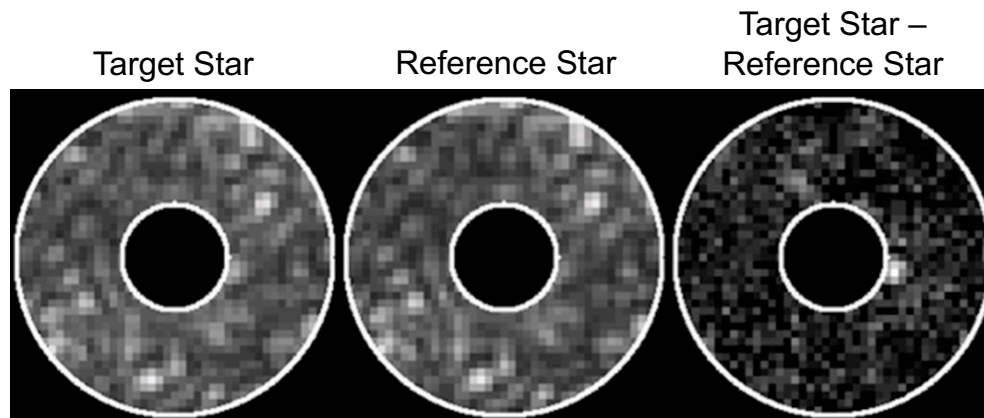
^aCalifornia Institute of Technology, Jet Propulsion Laboratory, Pasadena, California, United States

^bAmazon, Project Kuiper, Northridge, California, United States

^cTellus1 Scientific, LLC, Madison, Alabama, United States

JATIS 9(4) (2023)

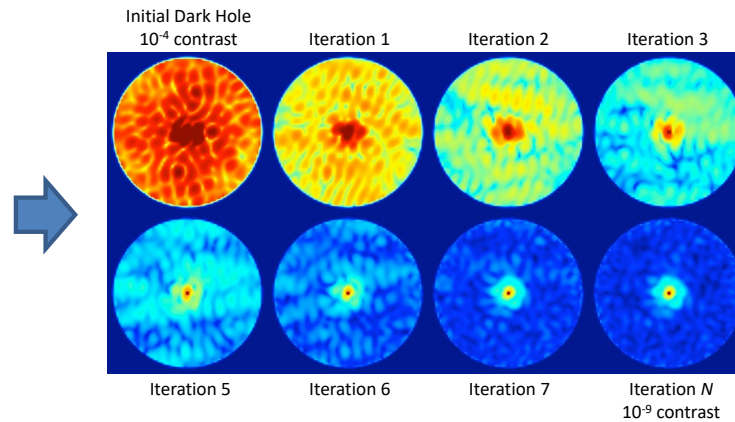
- Evaluate post-processing techniques (e.g., RDI, ADI, KLIP)
 - These will be used to recover embedded exoplanets and circumstellar disks
- Verify the CGI error budget
 - Predicts dark hole changes analytically using model-derived sensitivities to allocate performance requirements



- Diffraction model (including LOWFS)
 - Computes the dark hole by propagating the wavefront through the system model using Fourier-based algorithms
- STOP model
 - Structural, Thermal, and Optical Performance
 - Finite-element modeling of thermally-induced structural deformations
 - Ray tracing to derive resulting wavefront changes
- Dynamics model
 - Structural perturbations induced by reaction wheel vibrations
 - Primary effect is rapid pointing error (jitter)

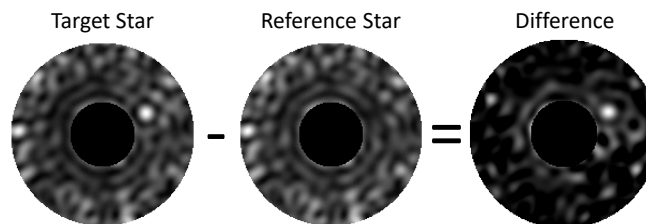
The Dark Hole

The initial dark hole:
The dark hole immediately
after running high-order
wavefront control



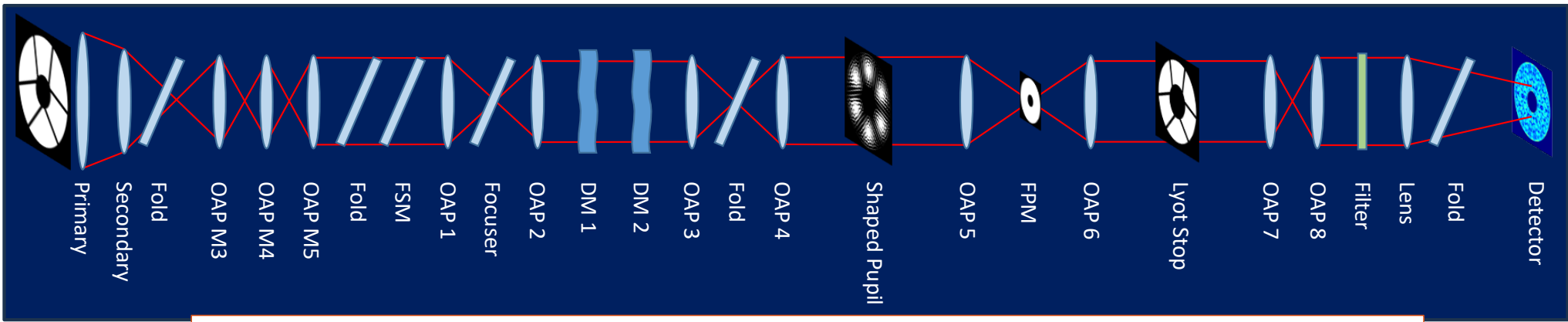
Modeled using:
Diffraction

The “dynamic” dark hole:
The dark hole as it varies
over time due



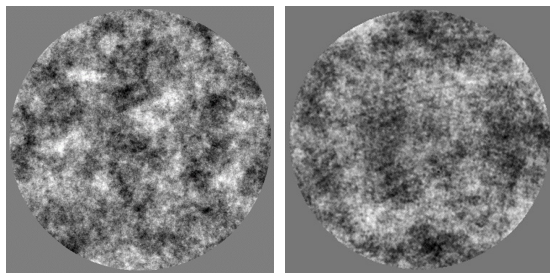
Modeled using:
STOP, pointing

Roman+CGI Unfolded Layout



Broadband image = multiple monochromatic images x 4 polarization components

Optic polishing errors



Synthetic

Measured

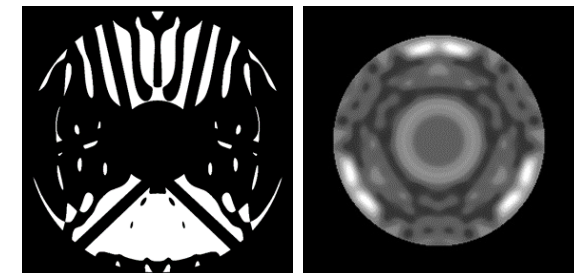
Polarization-dependent aberrations



Deformable mirrors



Masks



SPC pupil mask

HLC focal plane mask

CGI Wavefront Control

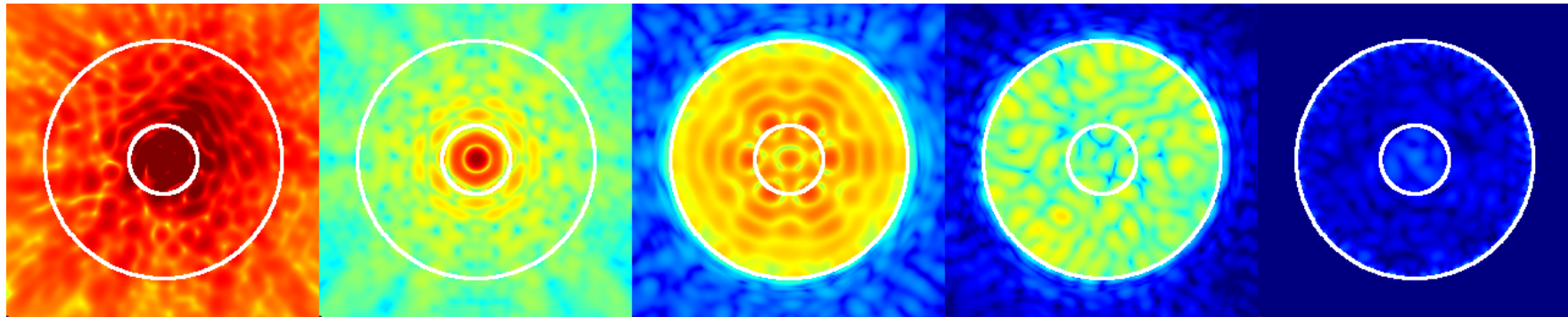
Contrast = 2×10^{-3}

4×10^{-6}

3×10^{-5}

2×10^{-6}

$\sim 10^{-9}$



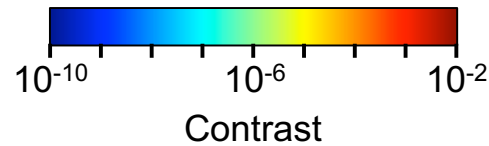
Before flattening
No HLC DM pattern
No masks

After flattening
No HLC DM pattern
No masks

After flattening
No HLC DM pattern
HLC masks

After flattening
HLC DM pattern
HLC masks

After HOWFS
HLC DM pattern
HLC masks



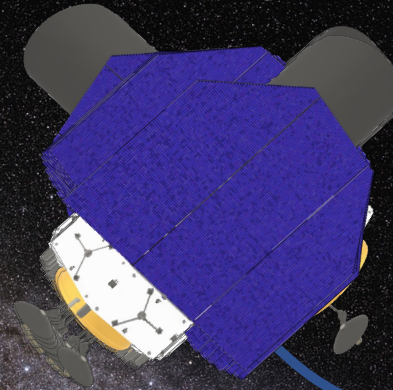
The same wavefront control algorithms are used in the models, testbeds, and on-orbit

CGI Observing Sequence

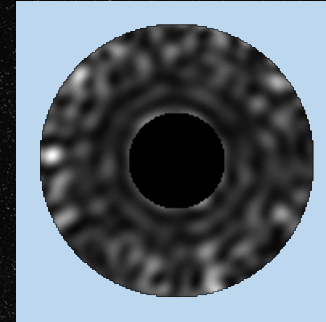
Bright Reference Star



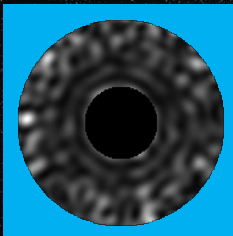
Target Star



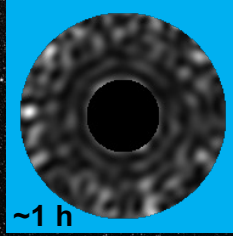
Reference star:
Target star:



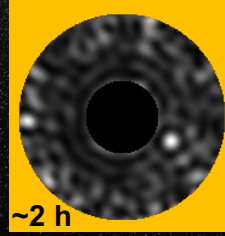
Dark hole



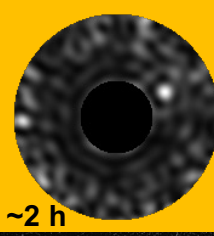
Reference image



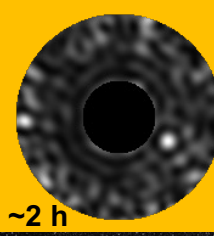
Target 0°



Target 23°



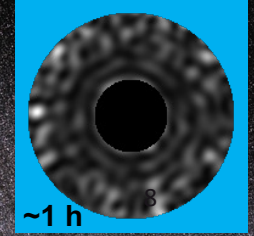
Target 0°



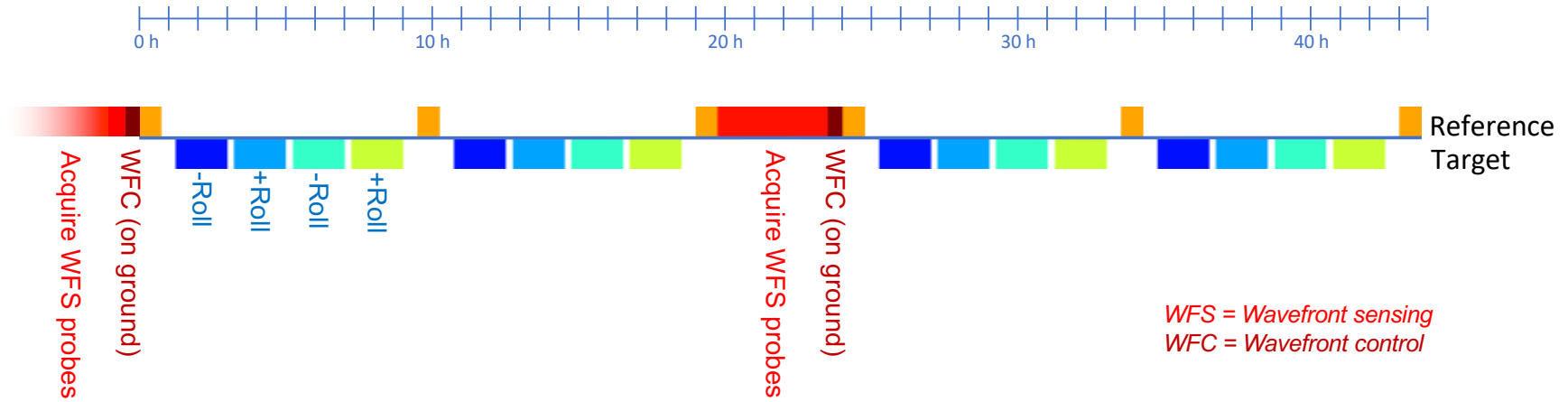
Target 23°



Reference image



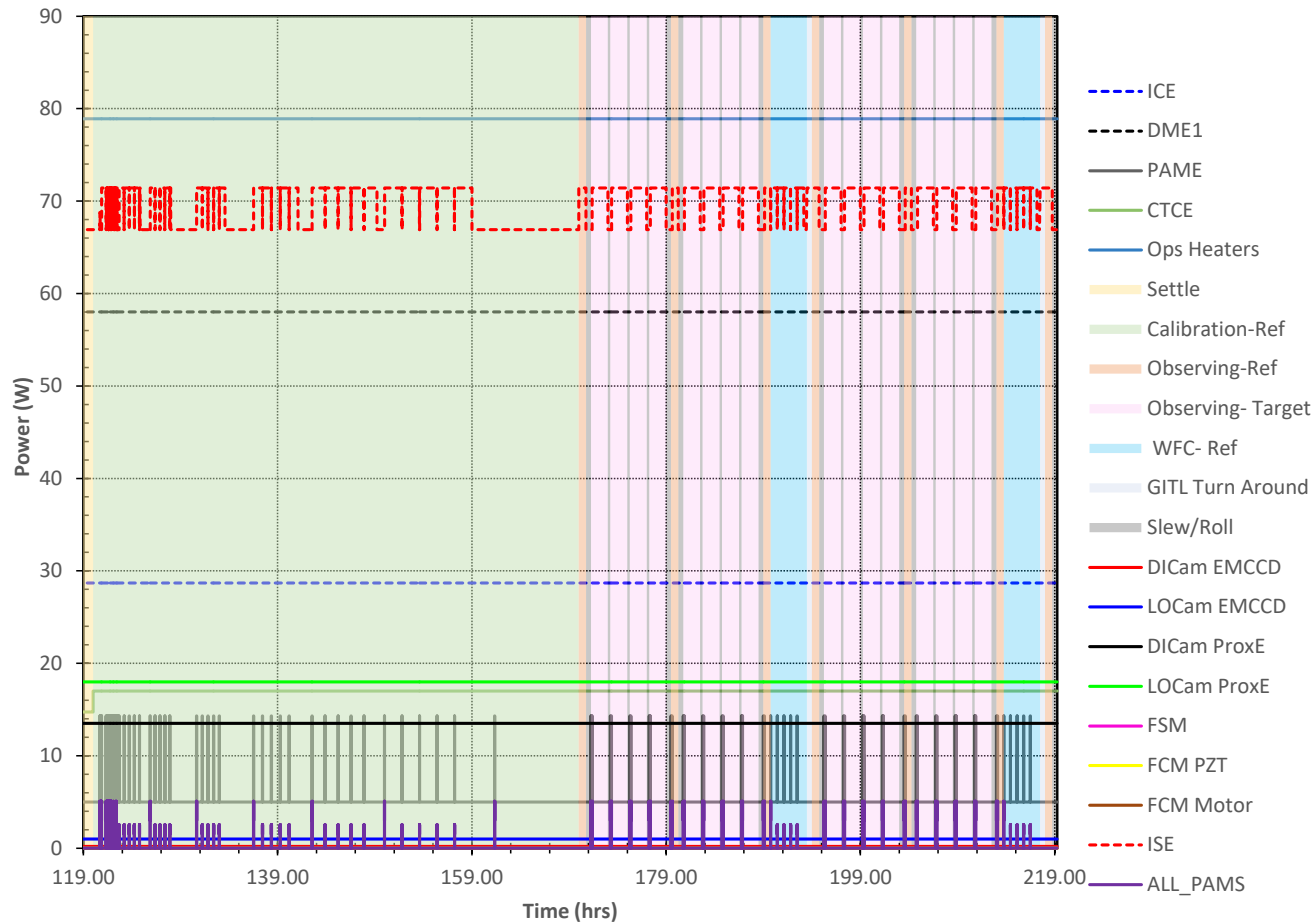
Observing Scenario 11 Timeline



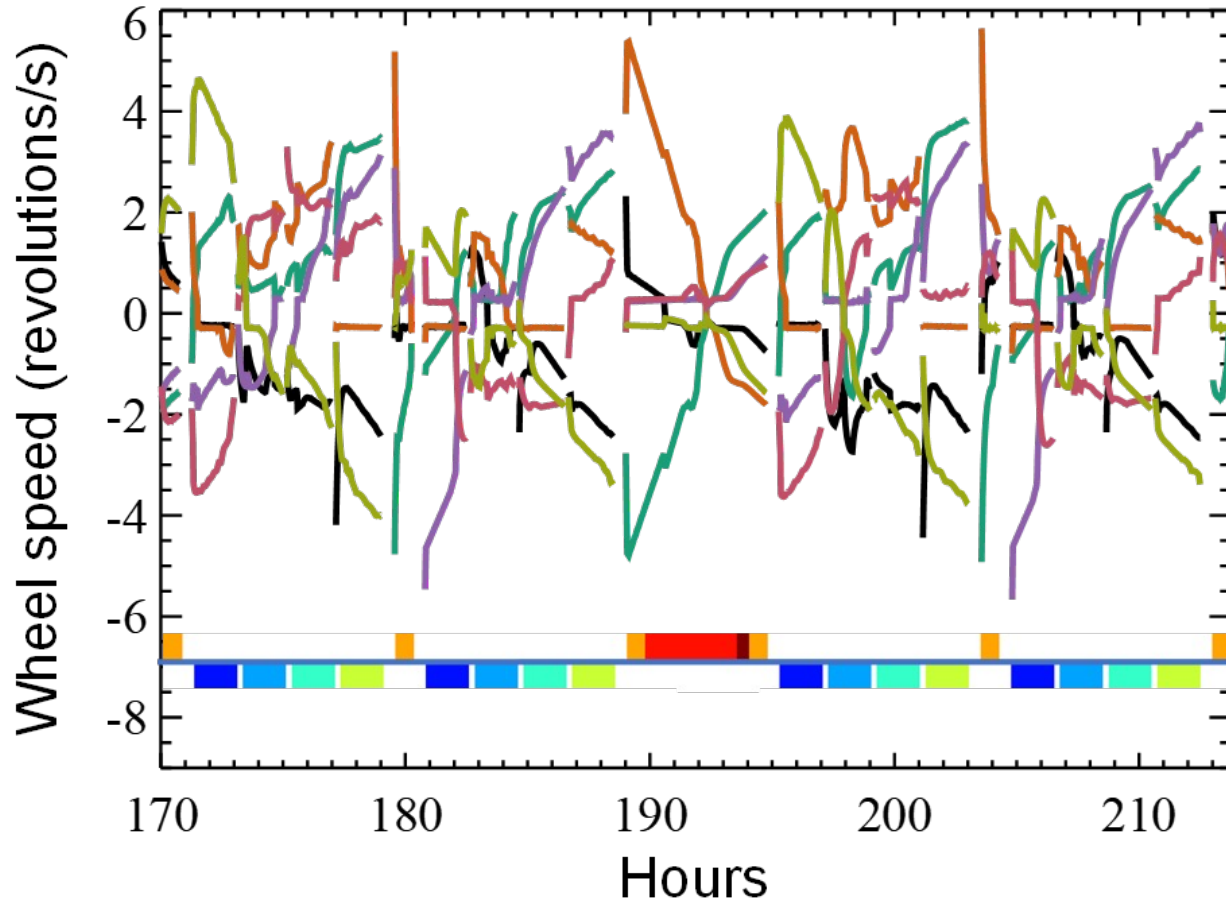
OS11 Orbital Parameters

	A	B	C	D	E	F	G	H	I	J	K	L	M	N	O
1	Times begin at 2026-05-21 00:00:00 UTC, sun moves as seen from Earth, locations are accurate at t in each line														
2	All positions are expressed as sequential (yaw, pitch, roll) right-handed rotations, with initial orientation aligning x (telescope boresight) toward the north ecliptic pole,														
3	Attitude Angles					Thermal Desktop Vectors									
4	Mode	Pointing	Time (hrs)	Yaw-θ_z (°)	Pitch-θ_y (°)	Roll-θ_x (°)	t [s]	x_sun	y_sun	z_sun	x_planet	y_planet	z_planet	r / r_planet	
5	Settle	HLS	0.00	125.5	-4.6	0.0	0	0.08	0.00	1.00	0.00	0.00	0.00	-1.00	20.00
6	Settle	HLS	120.00	125.5	-4.6	0.0	432001	0.08	0.00	1.00	0.00	0.00	0.00	-1.00	20.00
7	Calibration	zet Pup	120.50	-149.3	-8.3	10.3	433801	0.14	0.18	0.97	0.00	0.00	0.00	-1.00	20.00
8	Calibration	zet Pup	170.75	-149.6	-9.3	12.0	614700	0.16	0.21	0.97	0.00	0.00	0.00	-1.00	20.00
9	Observing	47 UMa	171.25	-58.7	-6.3	-12.5	616500	0.11	-0.21	0.97	0.00	0.00	0.00	-1.00	20.00
10	Observing	47 UMa	173.00	-58.7	-6.4	-12.5	622801	0.11	-0.22	0.97	0.00	0.00	0.00	-1.00	20.00
11	Observing	47 UMa	173.25	-58.7	-6.4	13.5	623701	0.11	0.23	0.97	0.00	0.00	0.00	-1.00	20.00
12	Observing	47 UMa	175.00	-58.7	-6.5	13.4	630001	0.11	0.23	0.97	0.00	0.00	0.00	-1.00	20.00
13	Observing	47 UMa	175.25	-58.7	-6.5	-12.6	630901	0.11	-0.22	0.97	0.00	0.00	0.00	-1.00	20.00
14	Observing	47 UMa	177.00	-58.7	-6.5	-12.6	637201	0.11	-0.22	0.97	0.00	0.00	0.00	-1.00	20.00
15	Observing	47 UMa	177.25	-58.7	-6.5	13.4	638101	0.11	0.23	0.97	0.00	0.00	0.00	-1.00	20.00
16	Observing	47 UMa	179.00	-58.7	-6.6	13.4	644401	0.11	0.23	0.97	0.00	0.00	0.00	-1.00	20.00
17	WFC	zet Pup	179.50	-149.7	-9.5	-13.7	646201	0.16	-0.23	0.96	0.00	0.00	0.00	-1.00	20.00
18	WFC	zet Pup	180.25	-149.7	-9.5	-13.7	648901	0.16	-0.23	0.96	0.00	0.00	0.00	-1.00	20.00
19	Observing	47 UMa	180.75	-58.7	-6.7	13.3	650701	0.12	0.23	0.97	0.00	0.00	0.00	-1.00	20.00
20	Observing	47 UMa	182.50	-58.7	-6.7	13.3	657000	0.12	0.23	0.97	0.00	0.00	0.00	-1.00	20.00
21	Observing	47 UMa	182.75	-58.7	-6.7	-12.7	657900	0.12	-0.22	0.97	0.00	0.00	0.00	-1.00	20.00
22	Observing	47 UMa	184.50	-58.7	-6.8	-12.8	664200	0.12	-0.22	0.97	0.00	0.00	0.00	-1.00	20.00
23	Observing	47 UMa	184.75	-58.7	-6.8	13.2	665100	0.12	0.23	0.97	0.00	0.00	0.00	-1.00	20.00
24	Observing	47 UMa	186.50	-58.7	-6.9	13.2	671400	0.12	0.23	0.97	0.00	0.00	0.00	-1.00	20.00
25	Observing	47 UMa	186.75	-58.7	-6.9	-12.8	672300	0.12	-0.22	0.97	0.00	0.00	0.00	-1.00	20.00
26	Observing	47 UMa	188.50	-58.7	-6.9	-12.8	678600	0.12	-0.22	0.97	0.00	0.00	0.00	-1.00	20.00
27	WFC	zet Pup	189.00	-149.7	-9.7	12.6	680400	0.17	0.22	0.96	0.00	0.00	0.00	-1.00	20.00
28	WFC	zet Pup	194.75	-149.7	-9.8	12.8	701102	0.17	0.22	0.96	0.00	0.00	0.00	-1.00	20.00
29	Observing	47 UMa	195.25	-58.7	-7.2	-13.0	702902	0.12	-0.22	0.97	0.00	0.00	0.00	-1.00	20.00
30	Observing	47 UMa	197.00	-58.7	-7.2	-13.0	709201	0.13	-0.22	0.97	0.00	0.00	0.00	-1.00	20.00
31	Observing	47 UMa	197.25	-58.7	-7.2	13.0	710101	0.13	0.22	0.97	0.00	0.00	0.00	-1.00	20.00
32	Observing	47 UMa	199.00	-58.7	-7.3	12.9	716401	0.13	0.22	0.97	0.00	0.00	0.00	-1.00	20.00

OS11 CGI Power Profile

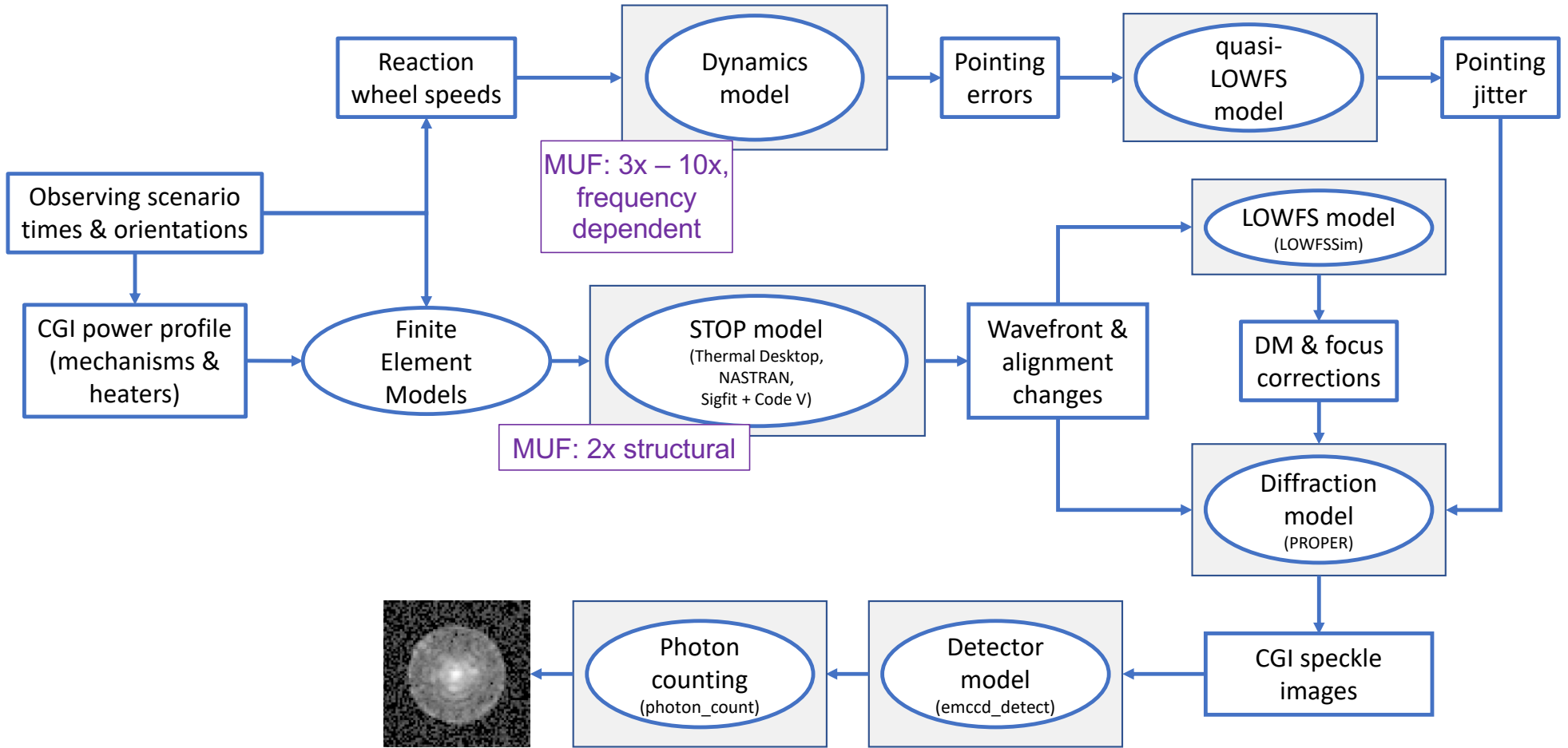


OS11 Reaction Wheel Speeds

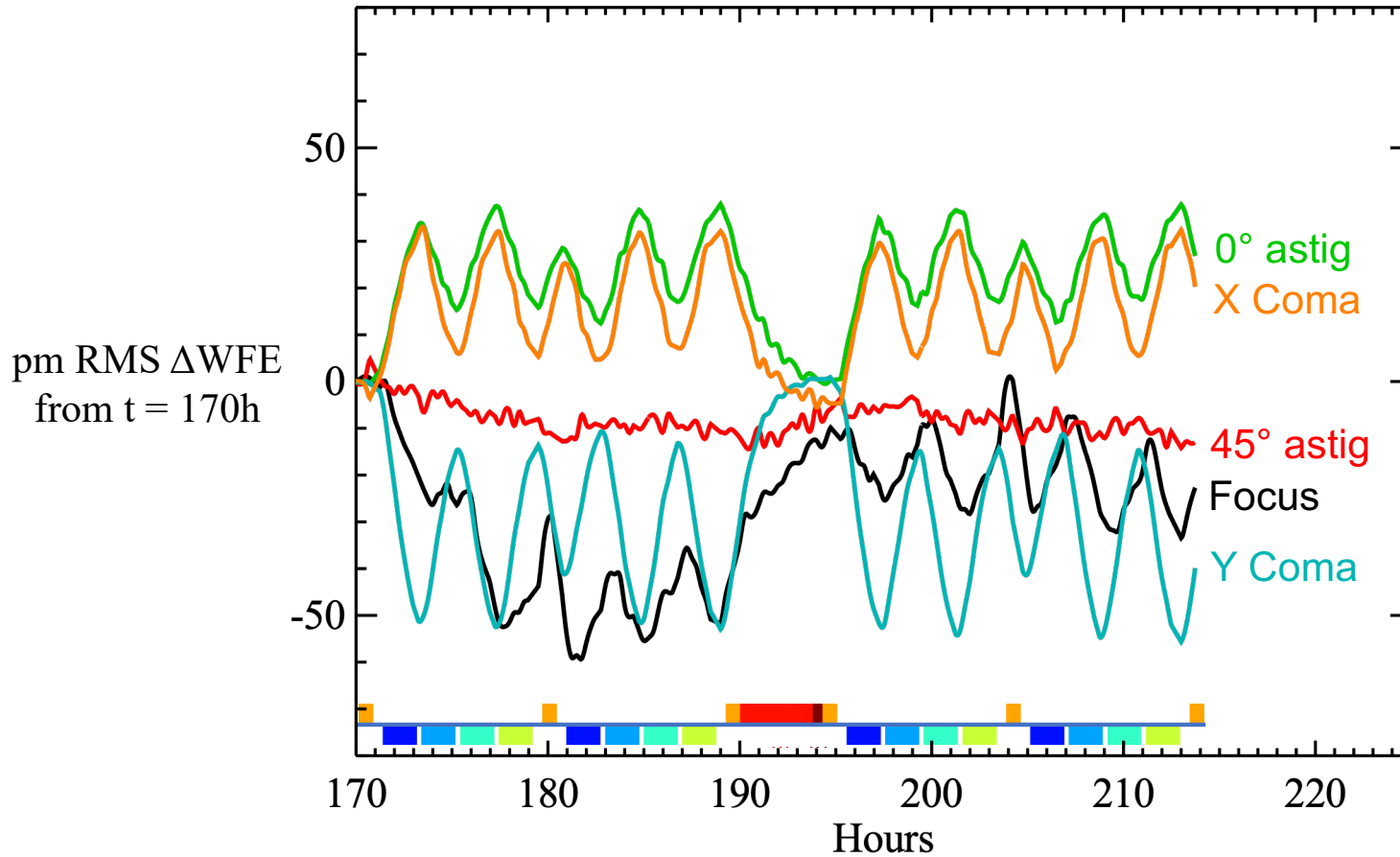


*~30 min to slew
~15 min to roll*

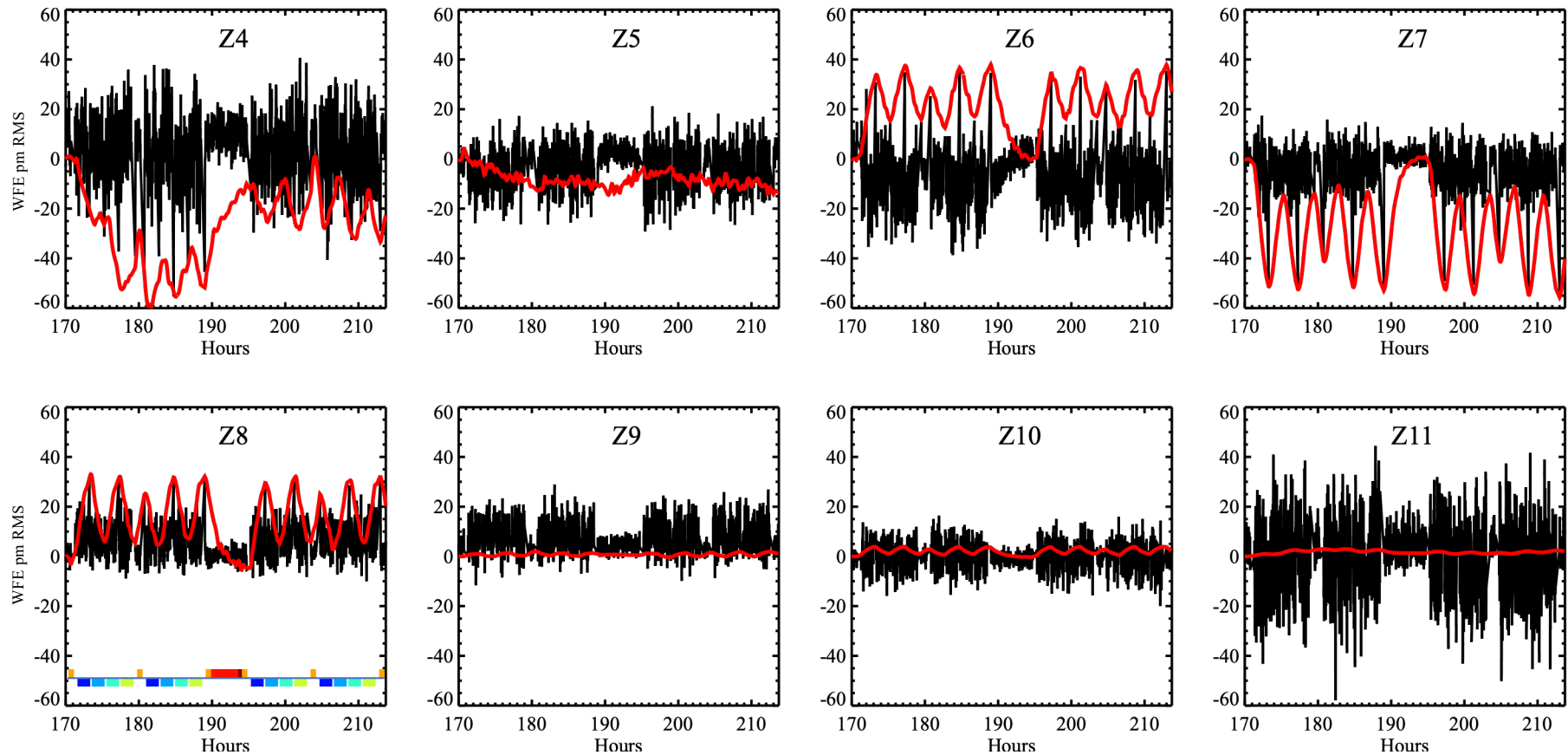
OS Time Series Computation Process



OS11 Low-Order Aberration Variations (before LOWFS correction)

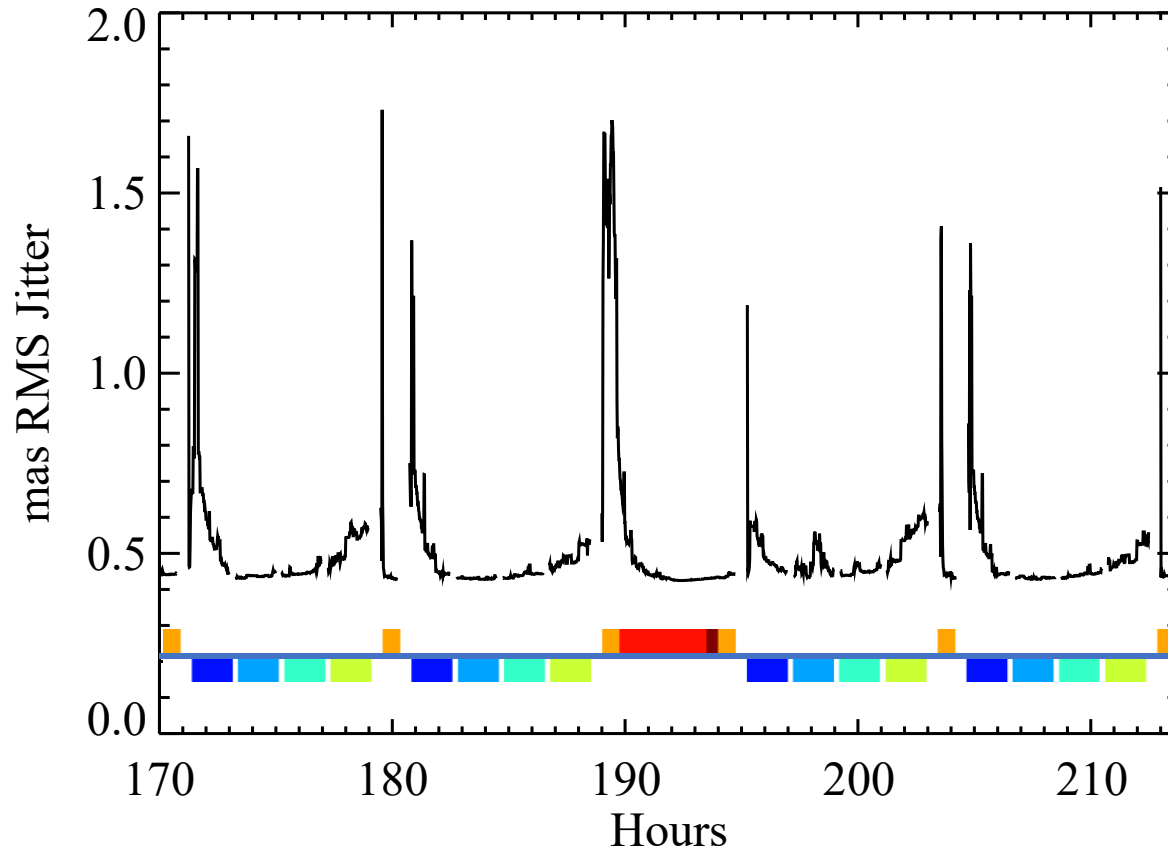


OS11 Low-Order Aberration Variations (after LOWFS correction on DM1)

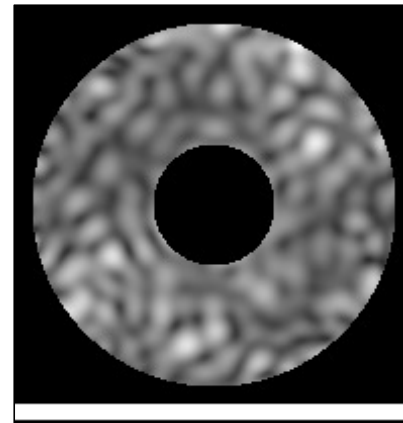


red = STOP-computed zernikes, black = LOWFS-corrected zernikes (1 m timesteps)

OS11 Pointing Jitter (after Fast Steering Mirror correction)



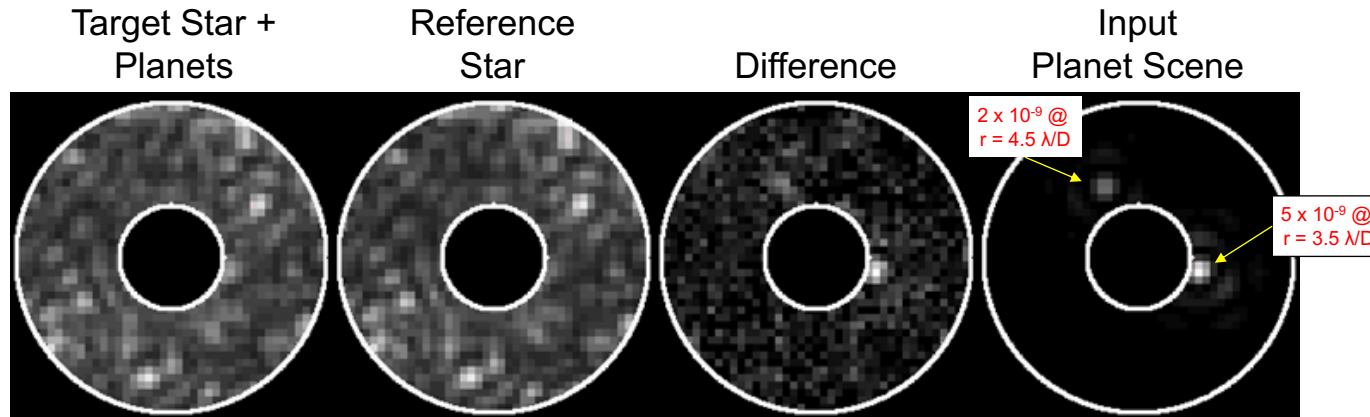
OS11 HLC Band 1 Results



0h 44h

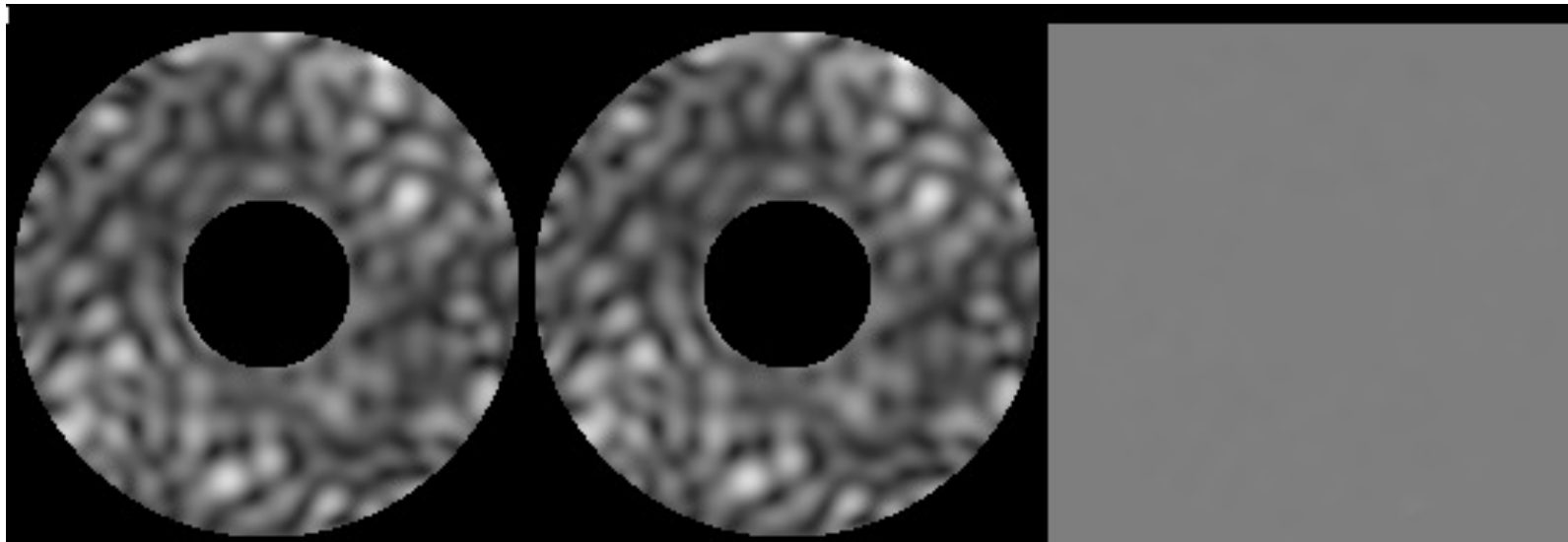
CGI OS11 Speckle Time Series
HLC Band 1
(no detector noise)

Time series available from:
<https://roman.ipac.caltech.edu/sims>



0h

44h



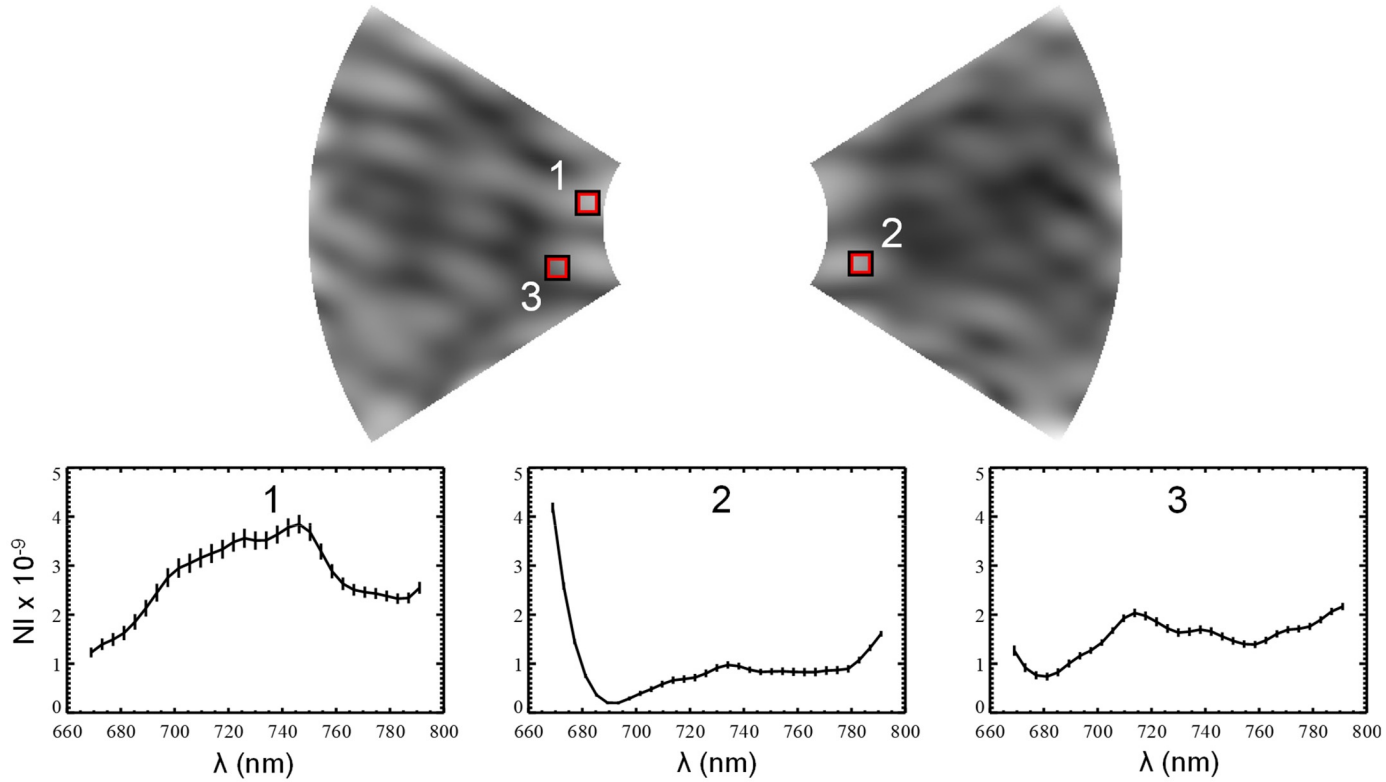
No LOWFS

With LOWFS

Difference

Jitter not included

OS11 SPC-Spec Band 3 Results



Error bars show intensity variation relative to mean over OS11

OS11 HLC Postprocessing Gains

Post-Processing Method	Noiseless			Noisy		
	5σ contrast	Gain	FAC	5σ contrast	Gain	FAC
No MUFs						
No sub., single roll minus	1.0×10^{-8}			1.3×10^{-8}		
No sub., single roll plus	1.0×10^{-8}			1.3×10^{-8}		
No sub., roll combined	8.0×10^{-9}			9.6×10^{-9}		
cRDI, single roll	2.2×10^{-9}	4.7		8.7×10^{-9}	1.5	
cRDI, roll combined	1.5×10^{-9}	5.3	1.2	6.1×10^{-9}	1.6	1.1
cADI, roll combined	6.2×10^{-10}	12.8	2.6	7.7×10^{-9}	1.3	0.9
KLIP RDI, roll combined	1.2×10^{-9}	8.3	1.7	5.9×10^{-9}	2.0	1.4
With MUFs						
No sub., single roll minus	2.7×10^{-8}			2.9×10^{-8}		
No sub., single roll plus	2.7×10^{-8}			3.0×10^{-8}		
No sub., roll combined	2.1×10^{-8}			2.2×10^{-8}		
cRDI, single roll	3.6×10^{-9}	7.4		1.3×10^{-8}	2.3	
cRDI, roll combined	2.5×10^{-9}	8.4	1.1	8.5×10^{-9}	2.6	1.1
cADI, roll combined	1.1×10^{-9}	18.8	2.5	1.1×10^{-8}	2.0	0.9
KLIP RDI, roll combined	1.9×10^{-9}	14.3	1.9	8.1×10^{-9}	3.5	1.5

From Ygouf et al. "Roman Coronagraph Instrument Post Processing Report – OS11 HLC Distribution" (2024)

- The OS11 simulations show that the speckle stability is
 - worst for brief periods after slews when the reaction wheels are spinning down
 - otherwise dominated by residual coma, which is roll-dependent
 - may be improved by tuning the LOWFS for the lower wavefront changes compared to requirements
- Advanced post-processing techniques (e.g. KLIP) provide an improvement of up to 2x over classical RDI
 - the more unstable the system, the greater the improvement factor
- Error budget was verified using a previous OS
- OS11 time series are provided on roman.ipac.caltech.edu for the 3 base modes (HLC, SPC-Spec, SPC-WFOV)
- Revised OS11 coming? Maybe. I don't know.